3D Cerebral Cortical Morphometry in Autism: Increased Folding in Children and Adolescents in Frontal, Parietal, and Temporal Lobes

Suyash P. Awate[1,⋆], Lawrence Win[2], Paul Yushkevich[1], Robert T. Schultz[2], and James C. Gee[1]

[1] Penn Image Computing and Science Lab (PICSL), University of Pennsylvania
awate@mail.med.upenn.edu
[2] Center for Autism Research (CAR), Children's Hospital of Philadelphia, USA

Abstract. This paper presents a systematic evaluation of cortical folding, or complexity, in autism. It introduces two *novel measures* to analyze folding in a specific region of interest, which, unlike traditional measures, produce an intuitive easily-interpretable description of folding and inform the nature of folding change by incorporating local surface-patch orientation. This study reports *new* findings of *increased* cortical folding in autistics in the frontal, parietal, and temporal lobes, as compared to controls. These differences are stronger in children than adolescents. The paper validates part of the findings using the new measures based on comparisons with traditional measures. Unlike studies in the literature, this paper reports new findings, via a *fully 3D* folding analysis on all brain lobes, based on the consensus of virtually *all* 6 folding measures used (2 new, 4 traditional) via rigorous statistical *permutation testing*. In these ways, this paper not only strengthens some previous clinical findings, but also extends the state of the art in autism research.

1 Introduction

Autism is a serious neurodevelopmental disorder that causes a variety of cognitive deficits impairing social interaction and communication. A good understanding of the underlying neurobiological causes is absent. Mostly, brain morphometry in autism [1,2,3,4,5,6], revealing abnormalities in both gray matter (GM) and white matter (WM), has been restricted to volumetry of tissues, lobes, brain, etc. For instance, Carper *et al.* [2] found volumetric abnormalities in the frontal, temporal, and parietal lobes, and attributed this finding to the role of these lobes in normal behavioral function. Levitt *et al.* [7] create maps of 22 major sulci and report anatomical shifts for some sulci in frontal and temporal lobes. Nordahl *et al.* [8] report increased sulcal depths for autistic subjects in the operculum and the intraparietal sulcus using surface-based morphometry

⋆ The authors gratefully acknowledge the NIH support of this work through grants HD042974, HD046159, MH068066, NS045839, U19-HD35482, U54-MH066494-01.

D. Metaxas et al. (Eds.): MICCAI 2008, Part I, LNCS 5241, pp. 559–567, 2008.

(SBM). They found all abnormalities to be more pronounced in children than adolescents.

Studies on cortical folding, or complexity, in autism have received very little attention. The degree of cortical folding is actually closely tied to brain volume [9]. Qualitative, *visual scoring-based*, analyses by Piven *et al.* [10] and Bailey *et al.* [11] report irregularities in folding patterns in the form of polymicrogyria and hyperconvoluted temporal lobes. Polymicrogyria typically increases the irregularity of the GM-WM interface [12]. A recent *preliminary* study by Hardan *et al.* [13] reports increased gyrification on one 2D coronal slice anterior to the corpus callosum. They compute a gyrification index (GI) by *manually tracing* the outer and inner cortical 2D contours. They *hypothesize* that the increased cortical convolutions in autistics will be more pronounced in children than in adults, finding negative correlation between GI and the autistics' age.

Apart from GI, there are several other measures [14,15,16] to characterize different aspects of cortical folding. These include measures defined using the properties of individual cortical-surface patches (*local measures*) and measures designed to extract information from the entire cortical surface taken as a whole (*global measures*). While Batchelor *et al.* [15] use a subset of these measures to study folding in the developing human fetal brain (region-based folding computation), Tosun *et al.* [16] use another subset to quantify cortical folding in Parkinson-plus syndrome (voxel-based folding computation).

2 Materials and Methods

2.1 Clinical Cohort and MRI

The clinical cohort comprised 70 normal males and 90 autistic males, both divided into 3 age groups: (i) children: 7.5 to 12.5 years, (ii) adolescents: 12.5 to 19.5 years, and (iii) adults: 19.5 to 31 years. The age distributions in the corresponding normal and patient groups were well matched. The sample size, mean age (in years), and standard deviation of age (in years) for the *normal* groups were: (i) 20, 10.5, 1; (ii) 24, 15.9, 2.3; and (iii) 26, 25.6, 3.4; and for the *autistic* groups were: (i) 48, 10.3, 1.3; (ii) 32, 15.5, 1.9; and (iii) 10, 25.7, 3, respectively. MR images were acquired on a GE 1.5T scanner; sagittal SPGR; 2 NEX, 1.2mm^3; TR=24; flip angle=45; matrix=192x256; FOV=30cm; 124 slices.

2.2 Traditional Measures for Cortical Folding Analysis

This study employs the traditional cortical-folding measures to compare and validate the performance of the new measures introduced in the next section. Traditional measures, described as follows, can be difficult to interpret.

1. *Intrinsic curvature index* (ICI) [14]: counts hemispherical features by integrating across all surface patches with positive Gaussian curvature.

$$\mathrm{ICI}(\mathcal{M}) = \frac{1}{4\pi} \int_{m \in \mathcal{M}} \mathrm{G}^{+}(\mathrm{m})\, d\mathcal{M}, \tag{1}$$

where $G^+(m) = \max(K_{\min}(m)K_{\max}(m), 0)$; $K_{\min}$, $K_{\max}$ are the principal curvatures. Any local bump/pit with a hemispherical shape, irrespective of its size, increases ICI by 0.5. However, ICI *ignores* cylindrical and saddle-like patches that have non-positive Gaussian curvature. This separation of curved patches, although mathematically sound, makes ICI *difficult to interpret*.

2. *Mean curvature L2 norm* (MCN) [15]: counts hemispherical and cylindrical features by integrating the mean curvature across all surface patches:

$$\mathrm{MCN}(\mathcal{M}) = \left[\int_{m \in \mathcal{M}} H^2(m) d\mathcal{M} \right]^{0.5}, \tag{2}$$

where $H(m) = [K_{\min}(m) + K_{\max}(m)]/2$. However, similar to ICI, MCN *ignores* non-planar surface patches having saddle-like shapes ($H(m) = 0$), thereby complicating the semantics of its application to cortical folding.

3. *Convexity ratio* (CR): is a global measure of folding defined as the ratio of the areas of the surface and its convex hull. Increased convolution/gyrification will increase CR. CR generalizes GI to 3D.
4. *Isoperimetric ratio* (IPR): is a global measure of folding defined as the ratio of surface area to the enclosed volume to the power 2/3. Convoluted surfaces have increased IPRs. Both CR and IPR, being global measures, fail to probe deeply into the *local causes* for the changes in folding.

All aforementioned measures, furthermore, ignore the *orientation* of surface patches, e.g. they fail to distinguish a road surface with multiple bumps from another road where the bumps are replaced by potholes. The bumps and potholes on a surface might be compared to cortical gyri and sulci, respectively.

2.3 Novel Measures for Region-Based Cortical Folding Analysis

This section describes two novel measures to quantify the degree of cortical folding in a region of interest. These novel measures are based on Koenderink's seminal work in differential geometry [17], which completely characterizes local surface patches/neighborhoods in terms of their *shape index* and *curvedness*. While the shape index characterizes the orientation associated with a surface patch, i.e. concave, hyperbolic (saddle), or convex, curvedness quantifies the deviation of the surface patch from planarity. This systematic and intuitive *reparameterization* (shape index, curvedness) of the surface descriptors (principal curvatures) can lead to more meaningful studies of cortical folding.

The *shape index* $S(m)$, for a patch at point m on surface $\mathcal{M}$, is

$$S(m) = -\frac{2}{\pi} \arctan \frac{K_{\max}(m) + K_{\min}(m)}{K_{\max}(m) - K_{\min}(m)}. \tag{3}$$

For instance, (i) a patch on a sphere, which has the same curvature in all directions, has $S = 1$; (ii) a patch on a cylinder, which has no curvature along the axis of the cylinder, has $S = 0.5$; (iii) saddle-shaped patch, which is convex in one direction and concave in the orthogonal direction, has $S = 0$. The shape index changes sign based on the orientation (notion of inside versus outside) of

the surface, e.g. a cap ($S = 1$) and a cup ($S = -1$). The shape index is independent of the scale associated with the surface patch. In this way, the shape index informs the *type* of the patch and its *orientation* (see Figure 1(e)).

The *curvedness* for the surface patch at point m, which perfectly complements the information captured by the shape index, is

$$C(m) = [0.5(K^2_{\max}(m) + K^2_{\min}(m))]^{0.5} \tag{4}$$

and measures the deviation from flatness or planarity. Thus, more convoluted surface patches produce larger values of C. The curvedness is, however, sensitive to the scale associated with the surface patch. For instance, if lengths are scaled up by $\lambda > 1$, then the resulting surface patch now covers a smaller portion of the surface, thereby reducing $K_{\max}$ and $K_{\min}$ by a factor of λ. Extremely small patches have $C \to 0$; indeed, all sufficiently-small patches can be well approximated as being planar (corollary of the Taylor's theorem).

Based on this local parameterization of surface *patches* in terms of the shape index S and curvedness C, this paper proposes *two novel measures* to quantify folding characteristics of cortical-surface *regions*. These novel folding measures are, by design, *invariant to translation and rotation* (changes in the location or orientation of the slice planes during MRI) as well as the scale (changes in the resolution of the MR image) of the cortical surface representation (akin to measures in previous section).

1. **Average curvedness** (AC)**:** We define AC by integrating the curvedness over the region of interest $\mathcal{M}$ on the cortical surface.

$$\mathrm{AC}(\mathcal{M}) = \left[\int_{m \in \mathcal{M}} C^2(m) d\mathcal{M} \right]^{0.5}, \tag{5}$$

   where $d\mathcal{M}$ is the area measure of a small surface patch. AC is *invariant to scale* because $C^2 d\mathcal{M}$ is invariant to scale. Planar surface patches do not contribute to AC. A *more-convoluted* cortex produces a *larger* value of AC.
2. **Average shape index** (AS)**:** We define AS by integrating the shape index over the region of interest $\mathcal{M}$ on the cortical surface

$$\mathrm{AS}(\mathcal{M}) = \int_{m \in \mathcal{M}} \mathrm{S(m)} \; \frac{d\mathcal{M}}{\| \, d\mathcal{M} \, \|}. \tag{6}$$

   AS measures the average convexity/concavity of a surface. Planar components of a surface do *not* contribute to AS. For example, a surface having more number of (convex) *bumps/protrusions* or larger protrusions will produce a *larger* AS. On the other hand, a surface having more number of (concave) *pits* will produce a *smaller* AS. The protrusions and pits on a surface might be compared to gyri and sulci on the cerebral cortex, respectively.

2.4 Folding Analysis in a Level-Set Framework

The basic components of the pipeline, described as follows, are shown in Figure 1.

Brain Tissue Segmentation: The skull stripping and initial alignment of the images into AC-PC space were performed manually using Analyze (Figure 1(a)).

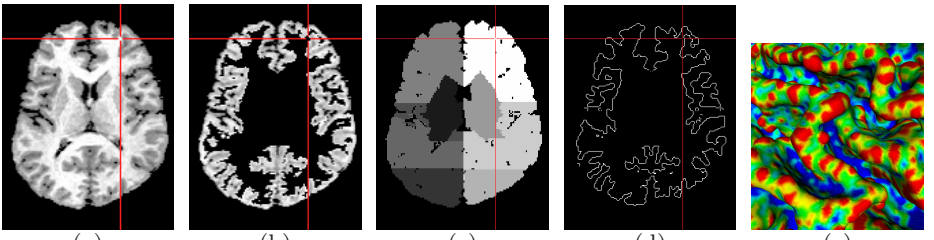

Fig. 1. (a) MR image, after skull stripping and CSF removal, showing GM and WM only. (b) Segmentation (only cortical GM shown) after labor-intensive manual editing of the WM-GM interface. (c) Parcellation of the GM+WM mask into lobes and subcortical region. (d) The cortical surface shown as a zero crossing of a level set (level-set embedding not shown). Note that the cortical surface is stored at a much higher resolution (0.4mm^3) as compared to (a)–(c) (1.2mm^3); so the view in (d) is an interpolated view at approximately the same slice as that in (a)–(c). (e) A visualization of the shape index computed at each point on a small part of the cortical surface. (red $\equiv$ convex, blue $\equiv$ concave, and yellow/green $\equiv$ hyperbolic/saddle-like patch).

Cerebrospinal fluid (CSF) was removed by thresholding prior to the automatic *binary* GM segmentation by the method developed by Zeng *et al.* [18]. Although this segmentation method [18] has been shown in one comparison to be the most sensitive and accurate of more than half dozen such algorithms [19], it is imperfect. Thus, in a slice-by-slice manner (across 3 orthogonal views), an expert amongst us *manually* corrected the cortical GM-WM interface returned from the automated procedure. This allowed for extremely accurate measurements of the inner cortical surface (Figure 1(b)) (intraclass correlation coefficients for all component ROIs exceed 0.9). We use these binary segmentations, as initial segmentations to the method developed by Awate *et al.* [20,21], to produce accurate probabilistic/fuzzy tissue segmentations.

Brain Parcellation into Lobes: A standard procedure was employed to manually (expert) delineate the boundaries of the lobes in both hemispheres. The lobes are the regions of interest for the study in this paper (Figure 1(c)).

Cortical Surface Delineation: Typical clinical MR images, with limitations on resolution and the ensuing partial-volume effects, provide significantly better contrast at the GM-WM interface (inner cortical surface) than the GM-CSF interface (outer cortical surface). Consequently, some SBM studies [14] select the mid-cortical surface manually. Some SBM approaches estimate the outer cortical surface relying on the accuracy of the inner cortical surface and assuming that the outer cortical surface has a similar shape as the inner one. Subsequently, they select the mid-cortical surface [8] which is even more similar to the inner cortical surface than the outer surface.

The lobe-specific study in this paper treats the inner cortical-surface contour that corresponds to a GM membership of 0.5 as the fiducial surface (similar to the approach in [15]) in order to achieve reliable and clinically-relevant results.

Conducting this lobe-specific folding study on the outer- or mid-cortical surface, instead, *may not alter current findings* because: (i) clinical evidence shows that polymicrogyria specifically affects the inner cortical surface, increasing its irregularity [12], (ii) an estimated outer/mid cortical surface would have a similar shape as the inner one, (iii) all folding measures, being scale invariant, would be unaffected by isotropic changes in size, and (iv) the integration involved in computing lobe-based folding measures produces robust estimates.

Representing the Cortical Surface as a Level Set: Unlike typical methods that encode the cortical surface via an explicit mesh representation, we employ an implicit level-set representation [22]. To improve the accuracy of the distance map that embeds the cortical surface as the zero level set (Figure 1(d)), especially near adjacent sulci that can come quite close to each other, we first supersample the tissue segmentation maps/images to a high resolution (0.4mm^3) and then fit [22] a level set, to the cortical surface, to subvoxel accuracy.

Compute Folding Measures: For every lobe, we compute the novel and the traditional folding measures. The surface gradients and derivatives of the level set, used to compute the principal curvatures and area measures of the cortical-surface patches, are obtained via standard numerical schemes [22].

2.5 Statistical Analyses Via (Nonparametric) Permutation Testing

Typical statistical analyses use the (parametric) Student's t test [14,16], which assumes that the observations are *independent*. Permutation tests, on the other hand, are nonparametric and rely on the *less inclusive* assumption that the observations are *exchangeable*, thereby making the test more stringent. Under the permutation-test null hypothesis (both samples generated by one distribution), the independent and identically-distributed observations are exchangeable.

We performed one-tailed permutation testing (more stringent than the corresponding t tests) to test if the autistics exhibited higher values for novel and traditional cortical-folding measures, for every lobe. A larger AC implies a more convoluted surface, while a larger AS indicates a surface with more (convex) bumps/protrusions. The permutation-test *statistic* was the *difference of means* between the normal and autistic samples; $200,000$ permutations.

3 Results and Discussion

Significantly-Increased Folding in Children: P values and effect sizes (D) in Table 1 indicate that virtually all measures *consistently* inform significantly-increased folding in frontal, temporal, and parietal lobes in both hemispheres. Unlike traditional measures, increased AS informs that increased folding resulted from more *protrusions*, *not pits*, on the WM at the WM-GM interface. While the differences are most significant in frontal and parietal lobes, they are insignificant in the occipital lobe (not reported) at the $p = 0.05$ level. These results are consistent with the preliminary folding study (on one coronal slice) by Hardan *et al.* [13] and extend those findings to other brain regions.

Table 1. Children: Cohen's *effects sizes* (D) and permutation-test *p values* (P) for 6 folding measures. AC and AS are proposed novel measures; ICI, MCN, CR, IPR are traditional measures. D values indicate the separation of the distributions independent of sample size ($D < 0.2$ is low, $D > 0.8$ is large separation). * indicates $P \geq 0.10$.

	Lt. Parietal		Lt. Temporal		Lt. Frontal		Rt. Parietal		Rt. Temporal		Rt. Frontal	
	D	P	D	P	D	P	D	P	D	P	D	P
AC	0.72	0.002	0.44	0.04	0.65	0.009	1	0.0003	0.46	0.02	0.76	0.002
AS	0.61	0.001	0.34	0.02	0.60	0.002	0.64	0.0001	0.54	0.002	0.48	0.003
ICI	0.50	0.02	0.49	0.03	0.66	0.008	1	0.0001	0.71	0.0007	0.56	0.01
MCN	0.56	0.01	0.56	0.01	0.68	0.005	1	0.0001	0.72	0.0007	0.77	0.002
CR	0.84	0.0005	0.37	0.08	0.55	0.02	1.1	0.0001	1	0.0001	0.50	0.03
IPR	0.54	0.01	0.08	0.35*	0.92	0.0007	0.79	0.002	0.79	0.01	0.67	0.008

Table 2. Adolescents: Cohen's effects sizes (D) and permutation-test p values (P)

	Lt. Parietal		Lt. Temporal		Lt. Frontal		Rt. Parietal		Rt. Temporal		Rt. Frontal	
	D	P	D	P	D	P	D	P	D	P	D	P
AC	0.41	0.05	0.23	0.17*	0.70	0.005	0.56	0.02	0.44	0.05	0.59	0.01
AS	0.38	0.01	0.49	0.01	0.35	0.01	0.42	0.03	0.58	0.005	1	0.001
ICI	0.23	0.19*	0.22	0.18*	0.73	0.005	0.33	0.09	0.72	0.006	0.38	0.08
MCN	0.36	0.09	0.36	0.08	0.71	0.005	0.51	0.03	0.68	0.007	0.35	0.09
CR	0.58	0.01	0.33	0.10*	0.42	0.06	0.38	0.08	0.65	0.008	0.33	0.11*
IPR	0.44	0.05	0.29	0.13*	0.60	0.01	0.55	0.02	0.76	0.003	0.27	0.14*

Increased Folding in Adolescents: P values and effect sizes (D) in Table 2 indicate folding changes similar to those in children, but less significant overall. Most measures *consistently* inform significant, or close-to significant, increase in folding in all cases except the left temporal lobe. The differences were insignificant in the occipital lobe (not reported) at the $p = 0.05$ level. These findings are consistent with [13,8] where such differences were expected, but were found insignificant. Hardan *et al.* [13] also report that GI correlates negatively with autistics' age. In this way, these results extend previous research. Observe that many p values in this case are only slightly higher than 0.05 and the corresponding D values are not too low.

Adults: We found insignificant differences in adults, consistent with previous hypotheses/findings [13,8]. However, the autistic adult sample size (10) is small.

Age-Independent Comparison: Permutation tests comparing the entire normal sample to the entire autistic sample, irrespective of age, produced p values (not reported) for *all* measures in *all* lobes that were *consistently smaller* than the p values in tables 1 and 2, thus indicating most significant differences. This finding supports the claim that the close-to-significant findings ($0.05 < p < 0.1$) for adolescents may increase significance with larger sample sizes.

References

1. Courchesne, E., Press, G., Yeung-Courchesne, R.: Parietal lobe abnormalities deteced with MR in patients with infantile autism. Am. J. Rad. 160, 387–393 (1993)
2. Carper, R.A., Moses, P., Tigue, Z.D., Courchesne, E.: Cerebral lobes in autism: Early hyperplasia and abnormal age effects. NeuroImage 16(4), 1038–1051 (2002)
3. Aylward, E., Minshew, N., Field, K., Sparks, B., Singh, N.: Effects of age on brain volume and head circumference in autism. Neurology 59, 175–183 (2002)
4. Hardan, A., Muddasani, S., Vemulapalli, M., Keshavan, M., Minshew, N.: An MRI study of increased cortical thickness in autism. Am. J. Psych. 163(7), 1290–1292 (2006)
5. Neeley, E.S., Bigler, E.D., Krasny, L., Ozonoff, S., McMahon, W., Lainhart, J.E.: Quantitative temporal lobe differences: Autism distinguished from controls using classification and regression tree analysis. Brain and Develop. 29(7), 389–399 (2007)
6. Mostofsky, S., Burgess, M., Gidley-Larson, J.: Increased motor cortex white matter volume predicts motor impairment in autism. Brain 130, 2117–2122 (2007)
7. Levitt, J., Blanton, R., Smalley, S., Thompson, P., Guthrie, D., McCracken, J., Sadoun, T., Heinichen, L., Toga, A.: Cortical sulcal maps in autism. Cerebral Cortex 13(7), 728–735 (2003)
8. Nordahl, C., Dierker, D., Mostafavi, I., Schumann, C., Rivera, S., Amaral, D., Van-Essen, D.: Cortical folding abnormalities in autism revealed by surface-based morphometry. Journal of Neuroscience 27(43), 11725–11735 (2007)
9. Armstrong, E., Schleicher, A., Omran, H., Curtis, M., Zilles, K.: The ontogeny of human gyrification. Cerebral Cortex 5, 56–63 (1995)
10. Piven, J., Berthier, M., Starkstein, S., Nehme, E., Pearlson, G., Folstein, S.: Magnetic resonance imaging evidence for a defect of cerebral cortical development in autism. Am. J. Psych. 147, 734–739 (1990)
11. Bailey, A., Luthert, Dean, Harding, Janota, Montgomery, Rutter, Lantos: A clinicopathological study of autism. Brain 121(5), 889–905 (1998)
12. Sztriha, L., Guerrini, R., Harding, B., Stewart, F., Chelloug, N., Johansen, J.: Clinical, MRI, and pathological features of polymicrogyria in chromosome 22q11 deletion syndrome. Am. J. Med. Genetics 127(A), 313–317 (2004)
13. Hardan, A., Jou, R., Keshavan, Varma, Minshew, N.: Increased frontal cortical folding in autism: a preliminary MRI study. Psyc. Res. 131(3), 263–268 (2004)
14. Van-Essen, D., Drury, H.: Structural and functional analyses of human cerebral cortex using a surface-based ATLAS. J. Neuroscience 17(18), 7079–7102 (1997)
15. Batchelor, P.G., Castellano-Smith, A.D., Hill, D.L.G., Hawkes, D.J., Cox, T.C.S., Dean, A.F.: Measures of folding applied to the development of the human fetal brain. IEEE Trans. Medical Imaging 21(8), 953–965 (2002)
16. Tosun, D., Duchesne, S., Rolland, Y., Toga, A., Verin, M., Barillot, C.: 3D analysis of cortical morphometry in differential diagnosis of Parkinson's Plus Syndromes. In: Med. Imag. Comput. and Comp. Assist. Intervention, pp. 891–899 (2007)
17. Koenderink, J., van Doorn, A.: Surface shape and curvature scales. Image and Vision Computing 10(8), 557–565 (1992)
18. Zeng, X., Staib, L., Schultz, R., Duncan, J.: Segmentation and measurement of the cortex from 3D MR images using coupled surfaces propagation. IEEE Trans. Medical Imaging 18(10), 100–111 (1999)
19. Shattuck, D.W., Leahy, R.M.: Brainsuite: An automated cortical surface identification tool. Medical Image Analysis 6(2), 129–142 (2002)

20. Awate, S.P., Tasdizen, T., Foster, N.L., Whitaker, R.T.: Adaptive Markov modeling for mutual-information-based unsupervised MRI brain-tissue classification. Medical Image Analysis 10(5), 726–739 (2006)
21. Awate, S.P., Zhang, H., Gee, J.C.: A fuzzy, nonparametric segmentation framework for DTI and MRI analysis: With applications to DTI tract extraction. IEEE Trans. Med. Imag. 26(11), 1525–1536 (2007)
22. Osher, S., Paragios, N.: Geometric Level Set Methods in Imaging, Vision, and Graphics. Springer, Heidelberg (2003)